frontiers | Frontiers in Earth Science

TYPE Original Research
PUBLISHED 09 May 2023
DOI 10.3389/feart.2023.1147124

OPEN ACCESS

EDITED BY
Faming Huang,
Nanchang University, China

REVIEWED BY
Ren Jie Chin,
Tunku Abdul Rahman University, Malaysia
Xiaoshen Xie,
Xi'an University of Science and Technology, China

*CORRESPONDENCE
Jing Liu,
ljing58@126.com

RECEIVED 18 January 2023
ACCEPTED 12 April 2023
PUBLISHED 09 May 2023

CITATION
Han X-Y, Yang W-B, Gao T-X, Jia G-P and Liu J (2023), The effect of double-row wing bag sand barrier on wind prevention and sand fixation: wind tunnel simulation and field verification.
Front. Earth Sci. 11:1147124.
doi: 10.3389/feart.2023.1147124

The effect of double-row wing bag sand barrier on wind prevention and sand fixation: wind tunnel simulation and field verification

Xue-Ying Han[1,2], Wen-Bin Yang[3], Tian-Xiao Gao[1], Guang-Pu Jia[2] and Jing Liu[1]*

[1]College of Desert Control Science and Engineering, Inner Mongolia Agricultural University, Hohhot, China, [2]College of Life Science, Yulin University, Yulin, China, [3]Institute of Desertification Studies, Chinese Academy of Forestry, Beijing, China

Introduction: Most of the sand fixation technologies utilized locally and internationally are static or dynamic, making it challenging for a single sand fixation mode to function in a harsh environment. Therefore, the development of a sand fixation mode that combines resistance and consolidation has emerged as a trending topic in sand control research. Our team developed the wing bag sand barrier, which is a static and dynamic combination of sand fixation mode.

Methods: In this study, we examined the characteristics of airflow velocity field and sand resistance near double-row wing bag sand barrier under different wind conditions to screen out the optimal mode of wing bag sand barrier. The analyses were conducted under nine configuration modes through the wind tunnel simulation experiment and the field experiment.

Results: The inflection point of the airflow was always 5H on the windward side of the wing bag sand barrier, regardless of the wind speed. The protection range of the wing bag sand barrier with the same specifications was gradually weakened with the increase of the wind speed. However, there was an upward trend in both total sand accumulation and sand accumulation of each height layer. When the wind speed was slower than 8 m/s, the sand accumulation behind the barrier was mainly concentrated in the 0–10 cm height layer, and when the wind speed was 12 m/s, it was mainly concentrated in the 30–60 cm height layer. At the leeward side of the wing bag sand barrier, sand particles were rejected in the range of 0–30 cm; however, they were conducted in the range of 30–60 cm. The protective effect of the wing bag sand barrier simulated in the wind tunnel experiment was consistent with that of the field experiment.

Discussion: For a wind speed of slower than 6 m/s, the recommended specification for the field-installed wing bag sand barrier was 25 cm × 20 cm or 30 cm × 20 cm. The specifications 25 cm × 20 cm and 25 cm × 25 cm were recommended at an inlet wind speed of 8 m/s. When the wind speed was greater than 12 m/s, the recommended specifications were 25 cm × 25 cm, 25 cm × 20 cm, and 20 cm × 25 cm.

KEYWORDS

desertification, wing bag sand barrier, protection effect, wind tunnel simulation, Ulan Buh Desert

1 Introduction

China is one of the countries with the largest area of desertification in the world, covering around 2.7 million km^2, which accounts for 27% of the total land area. The desertification in China has severely threatened the country's ecological security and sustainable economic and social development activities. Wind erosion is one of the main forms of sandy desertification caused by wind-blown sand movement and is the main contributing factor to desertification in China. About 70% of the desertified area (1.832 million km^2) in China has been caused by wind erosion (Yang, 2016; Guo, 2021).

Frequent and severe wind and sand activities in arid and semi-arid areas have damaged roads, railways, power transmission towers, and farmland in these regions (Gao, 2022). The wind-sand disaster prevention system can be divided into three categories: mechanical, biological, and chemical. The mechanical sand control system is the leading wind-sand disaster prevention system owing to its low price, convenient construction, quick effect, and less environmental pollution (Wu et al., 2003; Qu et al., 2014). The sand barrier is also called a mechanical sand barrier or wind barrier and is one of the main engineering sand fixation measures (Sun et al., 2012; Han et al., 2021a). It is constructed on the sand surface using firewood, straw, clay, branches, slats, pebbles, and other materials (Wu, 2003; Li et al., 2022).

According to Neuman et al. (2013), the roughness elements on the surface can significantly reduce the transport and migration of fine-grained sediments under wind action. Hu et al. (2002) conducted a comprehensive study on the protection techniques for preventing highway sand disasters. They observed a 26.1%–71.3% decrease in sediment transport following setting up a mechanical sand barrier which led to an increase in the surface roughness by 40–88 times compared to the mobile dune (Hu et al., 2002). A study by Li J Y et al. (2020) found that mechanical sand barriers have a clear positive impact on sand fixation and control and can effectively reduce wind erosion and improve the ecological environment. In addition to mechanical sand barriers, there are other types of traditional sand barriers, such as grass-checkered sand barriers (Qiu, 2004; Xu et al., 2018; Wang et al., 2020; Wang et al., 2021), clay sand barriers (Chang et al., 2000; Liu, 2008), geotechnical sand barriers (Dong et al., 2007; Bai, 2009; Nie, 2012), living sand barriers (Miao et al., 2018; Wang et al., 2018), branch sand barriers (Meng et al., 2014; Shi et al., 2021; Liang et al., 2022) and gravel sand barriers (Zhang et al., 2012; Li et al., 2022). All these traditional sand barriers have good wind-proof and sand-fixing effects. However, the above-mentioned traditional sand barriers have many drawbacks, such as being vulnerable to various forms of damage, degrading readily, being difficult to construct, having short material life, being expensive, and having limited practical applications (Dong, 2004). Therefore, developing advanced and efficient sand-fixing materials without the aforementioned drawbacks is urgently required to replace the conventional sand-fixing materials employed in current wind-sand disaster prevention and control systems.

A static sand fixation approach is used in conventional sand fixation methods, such as grass-checkered sand barriers or clay and gravel. In conventional sand fixation methods, sand mobility is very strong, and the sand burial process is passive (Wu, 2009). Plant sand fixation methods are dynamic and have strict environmental requirements during planting; hence, they cannot be applied under harsh natural environments (Luo, 2005). Therefore, it is crucial to develop a low-cost sand fixation technology that can adapt to the fluidity of sand and collect sand *in situ*. In the future, dynamic and static sand fixation methods will be the key breakthrough direction of desertification control research.

Wing bag sand barrier is developed based on the conventional sand barrier and consists of dynamic and static sand-fixing methods deviating from the standard approach of the single sand-fixing mode concept of a mechanical sand barrier (Yang et al., 2017). It is a new type of sand barrier with wind and sand resistance properties and has multiple benefits, including long service life, resistance to aging, convenient construction, durability, and controllable porosity (Gao, 2021). In the wing bag sand barrier, a wing is attached to the traditional bag-shaped sand barrier that can fluctuate with the wind (Han et al., 2021b). The wing attached to the sand barrier can make the sand wind more resistant and slow it down layer by layer, which will cause sand to settle in the bottom bag. The wing can reduce the wind by fluctuating, which also improves its wind-proof and sand-fixing effects (Gao et al., 2019). Furthermore, the coast can be reduced by increasing the distance between the two rows of sand barriers. Unlike other sand barriers, the size and the height of the wing bag sand barrier can be adjusted according to the topography and wind speed, which are not subject to the specifications and materials of the wing bag sand barrier. The selection of materials for the wing bag depends entirely on the location of the barrier and the climatic zone, and both can influence the best protective effect.

At present, the wing bag sand barrier technology has International and Chinese patent authorization and the support for significant special achievement authentication from the Ministry of Science and Technology and the Inner Mongolia Science and Technology Office. Nevertheless, the optimum specifications required to achieve the best protective effect by the wing bag sand barrier under different wind conditions are still unknown. Therefore, the main purpose of this study is to determine the best combination mode between the wing bag sand barrier bottom pocket diameter and the wing height under different wind conditions. This study carried out the wind tunnel simulation, field measurement of airflow velocity, and sand resistance characteristics near the double-row wing bag sand barrier under nine configuration modes. Furthermore, the airflow movement law, the action law of wind sand flow under the action of wing bag sand barrier, and its sand resistance efficiency were also analyzed. The study provides new ideas and techniques that can be applied to prevent and control sand disasters, and the theoretical basis and data support for the application of wing bag sand barriers in the future.

2 Materials

The wing bag sand barrier was built using a biodegradable plant base as raw material, which is decomposed into

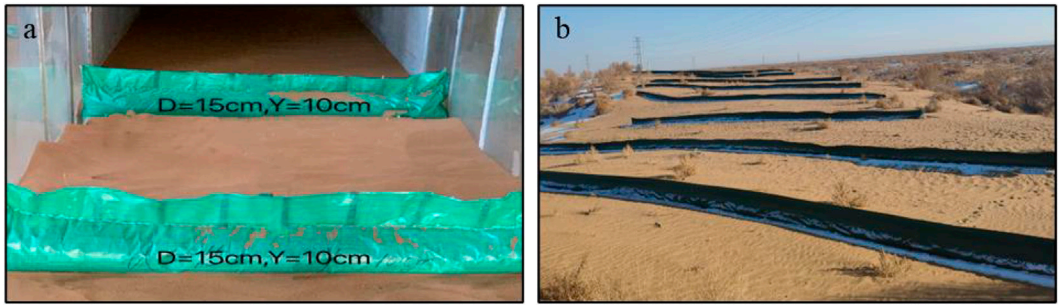

FIGURE 1
Experiment diagram of wing bag sand barrier. Note: **(A)** wind tunnel test chart, **(B)** field layout of wing bag sand barrier.

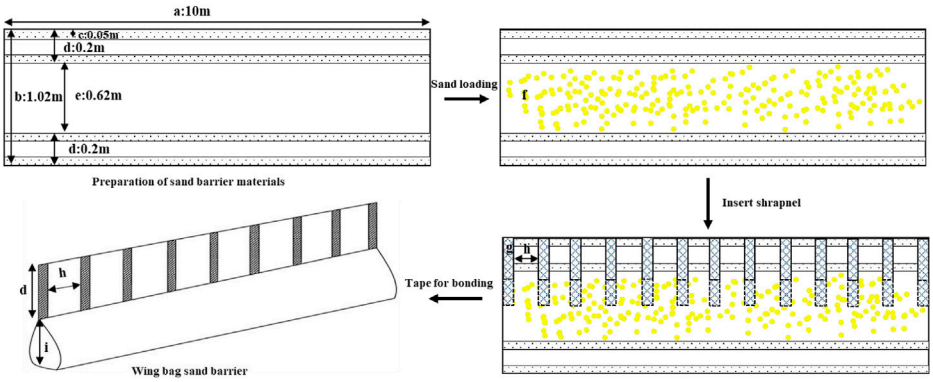

FIGURE 2
Wing sand barrier production flow chart (taking the size of 20 cm × 20 cm as an example). Note: **(A)** denotes the length of the material used (10 m), **(B)** denotes the width of the material used (1.02 m), **(C)** denotes reserve wing height (0.2 m), **(D)** denotes the width of the sticky bag (0.05 m), **(E)** denotes the circumference of the bottom belt (circumference 0.62 m), **(F)** denotes sand, **(G)** denotes the wing shrapnel which is made up with wire mesh (0.26 m × 0.05 m), **(H)** denotes width between two shrapnel (0.3 m), and **(I)** denotes the bottom band diameter (20 cm).

carbon dioxide and water by microorganisms in the soil. This is an environmentally friendly biological sand control material as it is non-toxic and does not cause pollution (Figure 1A). Based on the wind tunnel simulation the field test material was thickened, and weather and wind erosion resistivity were enhanced to better adapt to the harsh field environment (Figure 1B).

3 Methods

3.1 Construction and setting up of the wing bag sand barrier model

The wing bag sand barrier is a new type of combined sand barrier with two parts: the bottom bag and the wing. The bottom bag can fix the quicksand, and the wing can eliminate the wind by fluctuating. As a result, the conventional static sand fixation approach is transformed into a dynamic sand fixation. The field experiment was conducted at three bottom bag diameters (20 cm, 25 cm, 30 cm) and three wing heights (20 cm, 25 cm, 30 cm), with a total of nine configurations. A ratio of 1:2 (equal scale reduction) was employed between the wind tunnel simulation test and field-measured data to maintain comparability between the two data sets in the sand barrier model. For example, a 20 cm × 20 cm wing bag sand barrier was used in the modeling process (Figure 2). The dimensions of the material used in the sand barrier preparation were 10 m (Figure 2A) × 1.02 m (Figure 2B). Two 0.05-m adhesive strips were stitched on both ends of the material (Figure 2C), and the distance between the two adhesive strips was the wing height (Figure 2D). In the field construction, the sand barrier bottom belt (Figure 2E) was first irrigated before being filled with sand (Figure 2F) collected from the site. The sand content of the bottom belt exceeded 95% after joining the two rows of the adhesive belt. Secondly, the shrapnel (Figure 2G) was inserted up to 2/3 of the bottom pocket, and the top of the shrapnel was flush to the top of the adhesive tape to increase the wing strength. The spacing between the shrapnel (Figure 2H) was 0.3 m. Finally, the modeling was completed by gluing the double rows of adhesive tape. The wing bag sand barrier was simple to operate and implement in the field.

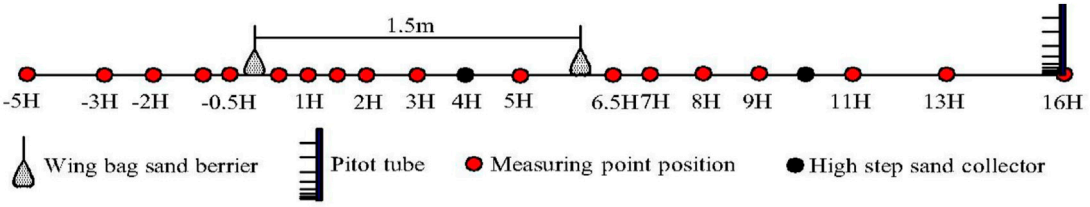

FIGURE 3
Layout diagram of measuring points of wind cup in the wind tunnel test.

3.2 Wind tunnel simulation experiment

The wind tunnel (Shapotou Soil Wind Tunnel Laboratory, Institute of Environment and Engineering in Cold and Arid Regions, Chinese Academy of Sciences) (Figure 1A) used in this experiment was initially built in 1990 and was expanded in 2003. It is a DC closed-blowing, low-speed tunnel and is composed of five parts: power section, rectifier section, sand supply device, experimental section, and diffusion section. The other features of the wind tunnel are as follows: the total length is 40 m, the length of the experimental section is 21 m, the cross-sectional area is 1.2 m × 1.2 m, and the thickness of the boundary layer is 50 cm. Wind speed can be adjusted continuously from 0 to 40 m/s. The experiment can be synchronized through the speed control module. The source and the particle characteristics of sand material do not impact the wind tunnel experiment of the wing bag sand barrier. The sand material used in the wind tunnel experiment was obtained from Tengger Desert, China.

The main topics of wind-sand physics research have always been the wind velocity profile and wind-sand flow structure. In this study, the wind velocity profile and wind-sand flow structure were changed at different points to reflect the effect of the wing bag sand barrier on preventing wind and sand. Specific observation points are as follows:

(1) Airspeed: The clean air free of sand and other impurities has nine modes of wind speed. Three wind speed grades of 6, 8, and 12 m/s were selected for the present experiment. Once the airflow was stabilized, the wind speed started to blow. The recording frequency and recording time of wind speed were 1 and 20 s, respectively. The wind speed was measured using a sand prevention wind speed profile and a pitot tube connected with a digital pressure acquisition instrument. The computer automatically recorded acquisition heights at 0.4, 0.8, 1.2, 1.6, 3.2, 6.4, 12, 20, 35, and 50 cm (Figure 3). The measuring points before the model were 0.5H, 1H, 2H, 3H, and 5H, and after the model were 0.5H, 1H, 1.5H, 2H, 2.5H, 3H, 4H, 4.5H, 0.5H, 1H, 2H, 3H, 5H, 7H, and 10H (H is the model height) (Figure 3).
(2) Aeolian sand flow: Without using a model, the aeolian sand flow was measured before and after the cavity under carrying wind and sand conditions. Three wind speeds applied were 6, 8, and 12 m/s, and the corresponding steady blowing times were 10, 5, and 3 min. The structure of aeolian sand flow was measured by a continuous equal-step sand collector. The aeolian sand flow observation position was 1 m behind each row of sand barrier (Figure 3). The sand collector had a height of 60 cm (60 layers) and a cross-section of 0.5 cm × 1 cm.

3.4 Sand barrier rejection rate/conductivity rate

The concept of rejection rate is proposed as it is assumed that the erosion process of surface sand is the superposition effect caused by pure wind shear stress and sand-bearing wind impact wear (McEwan and Willetts, 1993). That is, the number of eroded sand particles passed through the sand barrier can be calculated as the proportion of trapped/transported sand particles to the total sand. The formula is as follows (Eq. 1):

$$n = \frac{W - Q}{W} \times 100\% \quad (1)$$

Where, *n* is the sand barrier interception rate/conductivity; W is the open-air sediment transport flux at the same height, g/(cm^2·min); Q is the residual sediment transport flux after the influence of the sand barrier, g/(cm^2·min).

4 Results

4.1 Variation of the horizontal airflow velocity field in the wing bag sand barrier

The horizontal airflow field of the wing bag sand barrier was investigated under nine different configuration modes and three bandwidth spacing modes. After that, the optimal configuration mode and the layout spacing of the wing bag sand barrier were selected under various wind conditions.

4.1.1 Variation of the horizontal airflow velocity field of the wing bag sand barrier with different configurations

Figure 4 shows the horizontal airflow velocity field of the double-row wing bag sand barrier (distance 1.5 m) under wind speeds of 6, 8, and 12 m/s. The flow field characteristics of the wing bag sand barrier were similar under different configuration modes. The airflow started fluctuating at −5H, and the inflection point appeared at −2H. Due to the interference of the sand barrier, the lower airflow steadily raised, resulting in a strong airflow area at the top of the sand barrier. The wind speed decreased sharply when airflow passed through the barrier, and weak and calm wind regimes were developed inside and behind the barrier. The airflow returned to its original state as it moved away from the barrier.

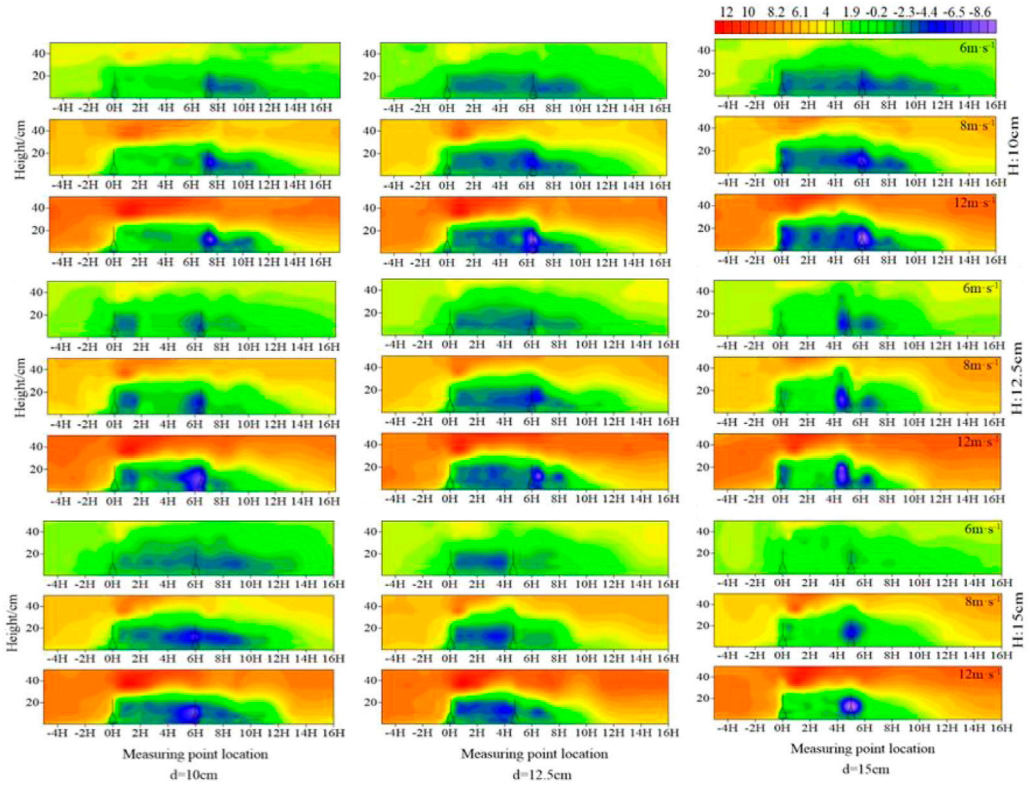

FIGURE 4
Horizontal airflow velocity field of wing bag sand barrier at different configuration modes.

TABLE 1 Comparison of the wind-proof effect of the sand barrier of wing bag of different specifications (indicating wind speed of 12 m/s).

Model specification (cm × cm)	WSBB ($m·s^{-1}$)	WSIB ($m·s^{-1}$)	WSAB ($m·s^{-1}$)	WE (%)
10 × 10	8.33	−1.60	3.59	70.08
10 × 12.5	8.16	−0.80	4.45	62.92
10 × 15	8.06	−2.40	2.01	83.25
12.5 × 10	7.83	−3.40	5.65	52.92
12.5 × 12.5	8.16	−3.20	5.2	56.67
12.5 × 15	8.06	−3.40	6.84	43.00
15 × 10	8.09	−4.00	5.00	58.33
15 × 12.5	8.21	0.90	7.13	40.58
15 × 15	8.19	−1.00	4.58	61.83

Note: WSBB, denotes the wind speed 5H before the barrier; WSIB, denotes the wind speed 4H in the barrier; WSAB, denotes the wind speed 10H after the barrier; WE, denotes the wind-proof efficiency.

In the same configuration mode, the protection range of the wing bag sand barrier was decreased by 2–4H with the increase in wind speed. However, the varying wind speed had little impact on the airflow field's variation. Also, the specific value of the disturbance effect of the wing on the wind speed was unaffected by the wind speed. The protection range of the nine configuration modes exceeded 16H when the wind speed was 6 m/s. For the wing bag sand barrier with specifications of 10 cm × 15 cm and 12.5 cm × 10 cm, the wind speed was only 2.78 and 3.24 m/s at the height of 50 cm of the measuring point within 16H. The inlet wind speed reached 8 m/s for three wing bag sand barrier specifications: 12.5 cm × 10 cm, 12.5 cm × 12.5 cm, and 10 cm × 15 cm. The thickness and protection distance of the static wind layer on the ground near the leeward side of the second-row sand barrier were better than those of the other configuration modes. When the wind speed was increased to 12 m/s and a wing height of 12.5 cm, the

10.3389/feart.2023.1147124

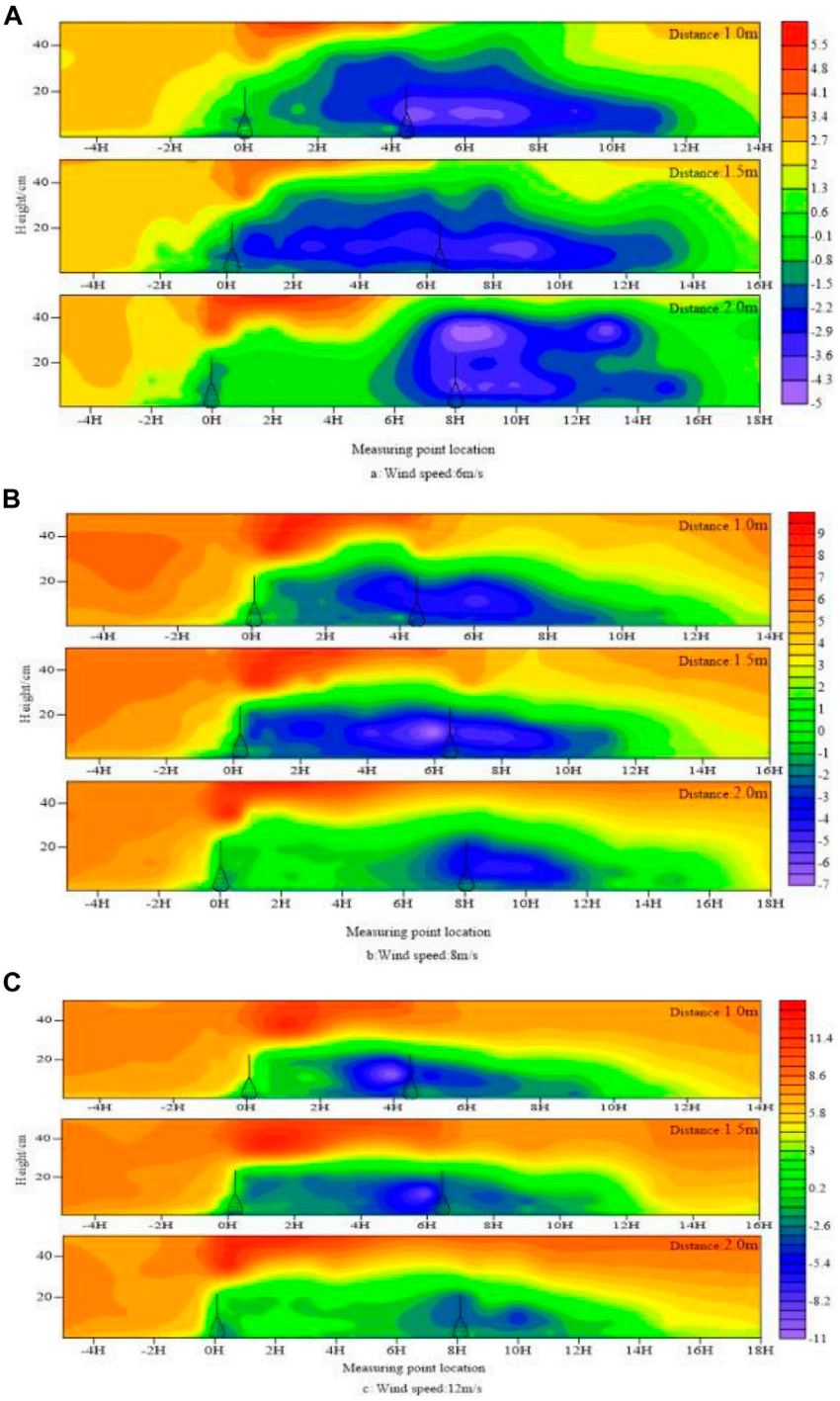

FIGURE 5
Horizontal airflow field diagram of wing bag sand barrier with different spacing.

protection range decreased in the order of 0–14H > 0–12 H for 12.5 cm × 12.5 cm sand barrier and > 0–10 H for 15 cm × 12.5 cm sand barrier. The results showed that at 12 m/s wind speed and constant wing height, the diameter of the bottom bag was inversely proportional to the protection range. Table 1 shows the wind-proof effect of the wing bag sand barrier with different specifications at a wind speed of 12 m/s. For the 10 × 15 wing bag sand barrier, the best protective effect of up to 83.25% occurred at a wind speed of 2.01 m/s at 10H and 0.2 m height on the leeward side. The wing bag sand barrier with a bottom belt diameter of 10 cm showed a better protective effect than those with other specifications. The wing bag sand barriers with specifications of 12.5 × 15 and 12 × 12.5 showed relatively poor (both less than 50%) protective effects, proving the size of the wing bag sand barrier had minimum impact on the protective effect.

TABLE 2 Protective range and area of wing bag sand barrier.

Model specification (cm × cm)	MS (m)	IWS (m/s)	B (H)	b (H)	PA (m^2)
10 × 15	1.0	6	2	>14	9.31
		8	1.5	14	7.05
		12	1	12.5	4.71
	1.5	6	2.5	>16	10.15
		8	2	14.5	7.32
		12	1	13	5.19
	2.0	6	2.5	>18	11.94
		8	2	18	7.88
		12	1	18	5.97

Note: MS, denotes the model spacing; IWS, denotes the indicated wind speed; B, denotes the effective protection distance before the barrier; b, denotes the effective protection distance behind the barrier; PA, denotes the effective protective area.

4.1.2 Variation of the horizontal airflow velocity field of the wing bag sand barrier at different spacing

The airflow field variation under different spacing was investigated by taking the wing bag sand barrier specification of 10 cm × 15 cm. Figure 5 shows the wind velocity diagram of the wing bag sand barrier with a distance of 1, 1.5, and 2 m under different wind speeds. At 6 m/s wind speed, the effective protection range after the barrier was 14H, 16H, and 18H for a distance of 1, 1.5, and 2 m, respectively.

The protection range at 8 m/s wind speed was 14H, 14.5H, and 18H, respectively, for the same distances, and when the wind speed increased to 12 m/s, the protection range was 12.5H, 13H, and 18H, respectively. Under the same wind speed, an increase in bandwidth spacing increased the protection range by 0.5–5H, and the protection area by 0.27–1.79 m^2 (Table 2). Under the same bandwidth, the increase of wind speed led to a decrease in the protection range before and after the barrier by 0.5–1.5H and 0–3H, respectively, and the protection area by 1.91–4.06 m^2, indicating a significant influence by bandwidth spacing while little impact by wind speed on the protection distance. The reduction of the protection area was mainly attributed to the gradual decrease in the thickness of the static wind layer above the surface. The best protective effect of the wing bag sand barrier was observed for a bandwidth of 2 m, followed by that of 1.5 m. The bandwidth of 1 m was too narrow, resulting in an overlap of the protective effect on the barrier, thereby generating a relatively weak protective effect.

4.2 Variation law of the vertical airflow velocity profile

The vertical airflow profile variation at various positions of the wing bag sand barrier with different specifications is shown in Figure 6. Figure 6A shows the vertical airflow profile of the wing bag sand barrier at a distance of 2 m and a specification of 10 cm × 12.5 cm under different wind speeds. The barrier settings used were: before the barrier (0.5H, 5H), in the barrier (0.5H, 4H), and after the barrier (0.5H, 7H). The vertical air velocity profile was unaffected by the wind speed, as shown by the negligible change of air velocity profile at three wind speeds and the same position of the wing bag sand barrier. Figure 6B shows the airflow profile variation of the wing bag sand barrier at various specifications and positions under one wind speed (12 m/s). The changes in the wind speed profile on both windward and leeward sides of the wing bag sand barrier were disturbed by varying degrees. The wind flow at the upwind side at −5H~−2H was not disturbed by the wing swing of the sand barrier. However, wind flow at the −1H~−0.5H fluctuated by varying degrees due to the influence of the sand barrier. The leeward airflow profile could be divided into three zones according to their shapes. In the first zone, the airflow velocity profile tended to have an “S” shape and was the best protection area, in which 0.5H–4H was the most affected by the sand barrier. The second zone was an airflow fluctuating area behind the barrier, and the airflow velocity profile tended to have an “S” shape in which 0.5H–7H is fluctuating state due to the influence of the sand barrier. The third zone was the airflow recovery area, and the airflow velocity profile tended to have a “semi-U” shape in which 10H was far away from the sand barrier and was not affected by the sand barrier.

In front of the barrier, the wind speed at 0–1H was increased by varying degrees with the increase in height. There, the airflow below 3 cm was significantly affected by the sand barrier. The average wind speed of nine wing bags was decreased to 5.01–6.49 m/s, among which the decrease of 10 cm × 10 cm was the most obvious. The acceleration process of the airflow was increased by 13%–32% with the increase in vertical height, and the most significant enhancement of the airflow was observed at the wing bag sand barrier specification of 12.5 cm × 12.5 cm. In the barrier, the airflow produced a strong vortex near both sides of the sand barrier due to the swinging of the wings. The velocity of the airflow was decreased when the vortex collided with the incoming airflow. The sand barrier had a noticeable impact when the wind was quiet, below 0.2 m, and in the range of 0–4H. At the wing bag sand barrier specification of 12.5 cm × 15 cm, the airflow in the range of 0–5H fluctuated by the sand barrier. However, the airflow greater than 7H was not affected by the sand barrier. The airflow velocity higher than 20 cm was not affected by the sand barrier and returned to the indicated wind speed.

10.3389/feart.2023.1147124

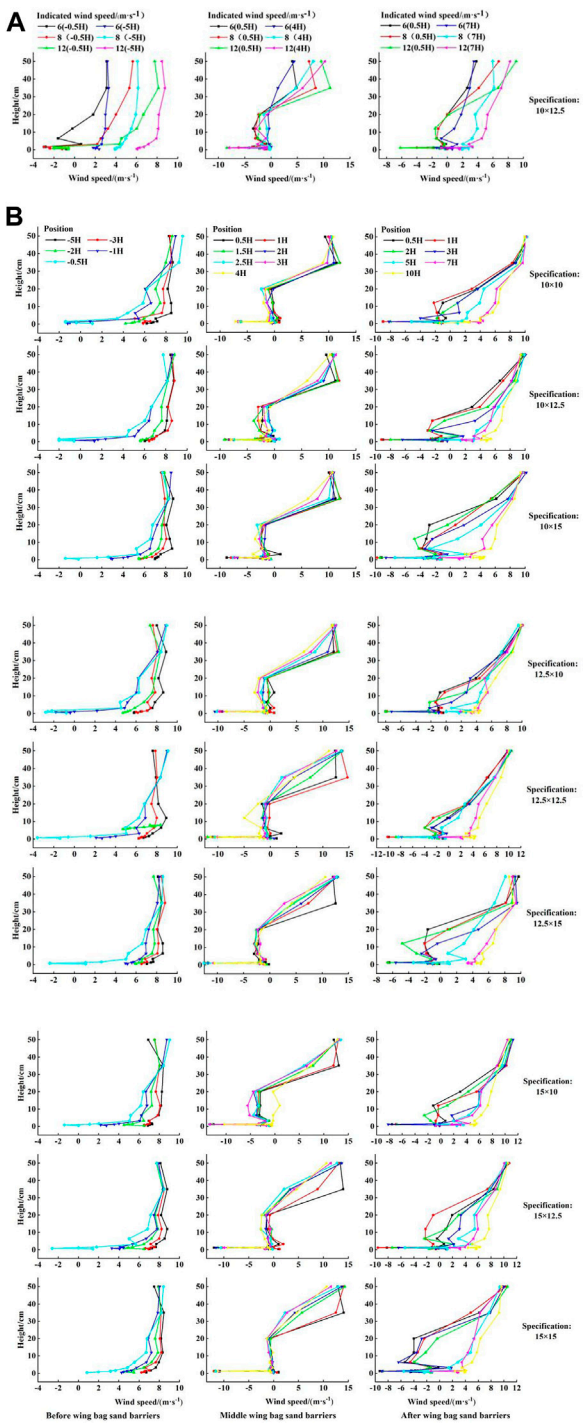

FIGURE 6
Air velocity profiles of different wing bag sand barriers.

4.3 Variation of the characteristics of wind sand flow structure

Under three wind speeds of 6, 8, and 12 m/s, the vertical distribution of wind-blown sand flow in the middle and 1 m behind the barrier at nine configuration modes of the double-row wing bag sand barrier is shown in Figure 7. The change in wind speed had a significant effect on sediment transport (Figure 7). The total sediment volumes under the wind speeds of 6, 8, and 12 m/s were 0.134 g·cm^{-2}·min^{-1}, 0.673 g·cm^{-2}·min^{-1}, and 4.274 g·cm^{-2}·min^{-1} respectively. In the 0–10 cm height layer behind the barrier, the sediment content accounted for 100%, 63%, and 31% of the total sediment content, respectively. In the 30–50 cm height layer, the sediment content accounted for 0%, 15%, and 16%, respectively, and in the 50–60 cm height layer, 0%, 21%, and 48%, respectively. At 6 and 8 m/s wind speeds, the deposited sand was mainly distributed in the 0–10 cm height layer. However, it was mainly distributed in the 50–60 cm height layer when the wind speed was 12 m/s. This was because the bottom of the bag of the sand barrier was sealed, and the swing of the wings disturbed the wind. Although the sand-carrying strong airflow can be blocked in a short time, it can be raised with a gradual increase in the wind speed. The specific gravity of sediment transport was gradually decreased at the height of 0–10 cm in the middle and behind the barrier, while that was steadily increased at the height of >10 cm. Table 3 shows the total amount of sand transport inside and after the sand barrier for different wing bag specifications at the wind speed of 12 m/s. The wing bag sand barriers with specifications of 10 × 10 and 10 × 15 had a relatively weak ability to reduce sediment transport. The wing bag sand barrier with the specification of 15 × 15 had the strongest ability to reduce sediment transport, which accounted for a reduction of 78.50%. The wing bag sand barriers with specifications of 12.5 × 15 and 15 × 12.5 decreased the sediment transport by 75.00% and 71.00%, respectively. The three bottom zone specifications (10 cm) cm showed a relatively weak ability to reduce sediment transport, indicating some degree of influence on sediment transport.

Table 4 shows the changes in interceptions/transmissibility on the leeward side of three wing bag sand barrier specifications with the bottom bag diameter of 12.5 cm at various heights and at wind speeds of 6, 8, and 12 m/s. The leeward side of the sand barrier functions as an interceptor in the 0–10 cm and 10–30 cm height layers and as a transporter in the 30–50 cm and 50–60 cm height layers. With the increase in wind speed, the interception rate in the 0–30 cm height layer decreased, while the conductivity in the 30–60 cm height layer increased. The interception rate increased with the wing height and was closer to 100% when the wind speed was 6 m/s. The increase in the wing height from 10 to 15 cm increased the interception rate of the sand barrier by 8% on average, mainly due to less amount of sand transported by the wind at low wind speed. When the wind speed increased to 12 m/s, the wing of the sand barrier appeared to be lopsided due to being in a higher position. Consequently, the interception effect of the wing bag sand barrier with the specification of 12.5 cm × 15 cm reduced (54%) at the height of 10–30 cm. At the height of 30–60 cm, the conduction effect was significant, and the average conductivity was 99%. At different wind speeds, the average interception rate at 0–30 cm height was 95%, and the conductivity rate at 30–60 cm height was 96%. Based on the results in Table 4, it is evident that the effect of the wing bag sand barrier with the specification of 12.5 cm × 15 cm was better than that of 12.5 cm × 15 cm and 12.5 cm × 10 cm.

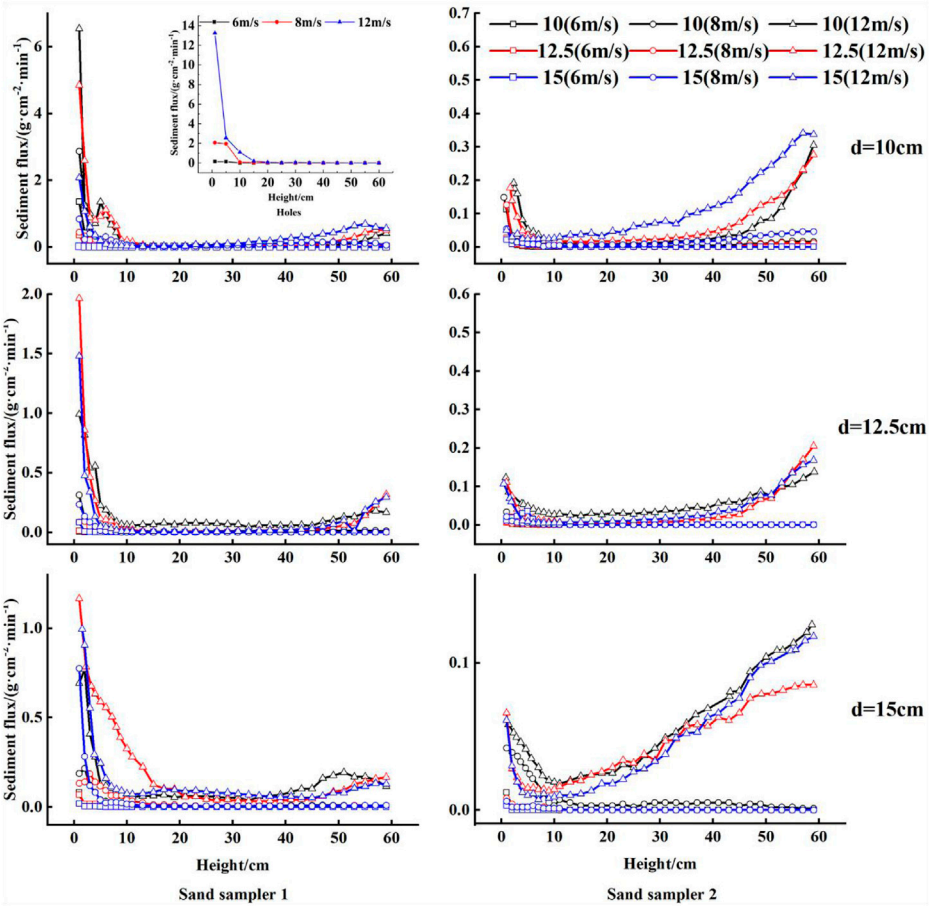

FIGURE 7
Vertical distribution of wind-blown sand flow on the wing bag sand barrier.

TABLE 3 Total sand transport of the wing bag sand barrier of different specifications (indicating wind speed 12 m/s).

Model specification (cm × cm)	TSTBB g/(cm²·min)	TSTAB g/(cm²·min)	RSD (%)
10 × 10	11.143	4.274	33.00
10 × 12.5	12.677	0.436	20.10
10 × 15	10.86	4.641	18.00
12.5 × 10	5.327	2.307	60.00
12.5 × 12.5	4.237	1.578	68.00
12.5 × 15	3.33	1.972	75.00
15 × 10	4.682	2.467	65.10
15 × 12.5	3.889	1.083	71.00
15 × 15	2.851	1.941	78.50

Notes: TSTBB, denotes the total sediment transport between barriers; TSTAB, denotes the total sediment transport behind the barrier; RSD, denotes the reduced sediment discharge.

4.4 Field effect evaluation

4.4.1 Study area

The study area is located in the Ulan Buh Desert in the south of the sand-crossing highway of Dengkou-Ejina Banner, China (40°22′19″- 40°22′35″ and 106°48′35″- 106°49′4″) (Figure 8). The surface wind erosion in the area is strong due to frequent wind and sand activities. The main wind direction is NW-WNW, and the annual sand wind frequency accounts for 54% with 85 annual wind sand days. The annual average and maximum wind velocities are

TABLE 4 Rejection rate/conducting rate of the wing bag sand barriers.

Indicated wind speed (m/s)	The height of the substratum (cm)	Model specification (cm × cm)		
		12.5 × 10	12.5 × 12.5	12.5 × 15
6	0–10	−94.02%	−95.87%	−94.79%
	10–30	−89.23%	−96.51%	−96.37%
	30–50	--	--	--
	50–60	--	--	--
8	0–10	−68.38%	−93.02%	−93.97%
	10–30	−89.03%	−95.34%	−80.75%
	30–50	+92.50%	+92.33%	+96.98%
	50–60	+94.26%	+95.64%	+95.88%
12	0–10	−39.32%	−91.95%	−70.82%
	10–30	−97.76%	−92.84%	−37.38%
	30–50	+94.35%	+96.56%	+99.08%
	50–60	+94.57%	+97.85%	+98.15%

Notes: − is the model rejection rate, + is the model conducting rate, -- represents no accumulated sand in this layer.

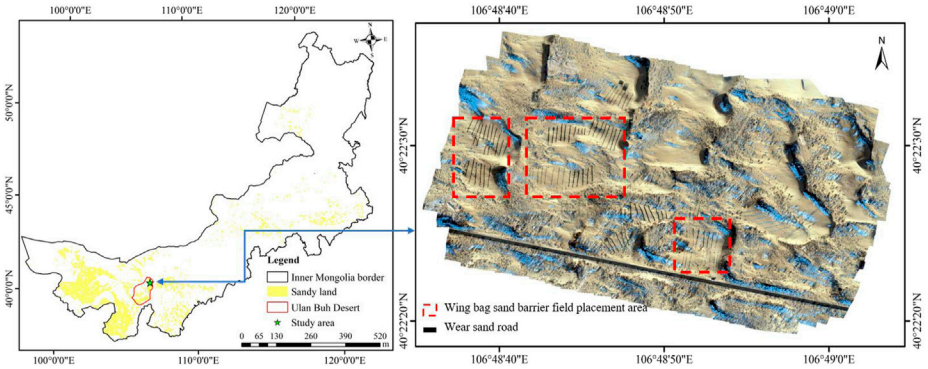

FIGURE 8
Geographical location of the study area.

3.7 and 21 m·s^{-1}, respectively. A large number of horizontal dunes and dune chains are distributed across the study area, with low surface vegetation coverage. The area has sufficient sand sources and strong wind power, which can provide dynamic conditions for wind-blown sand activities. Therefore, the study area is an ideal place to investigate the protective effects of sand control measures.

4.4.2 Measurement of field wind speed and flow field

A total of 15 wind speed values were measured at points in front of the sand barrier, in the middle of the barrier, behind the barrier, and in the wilderness using wind speed and direction collector (HOBO, United States). The measuring points were located at 4, 2, and 0.5 m in front of the barrier, at 0.5, 1.5, and 2.5 m in the middle of the barrier, and 1, 2, 3, 4, and 5 m behind the barrier. The control measuring points in the field were in the wilderness, and the heights of the wind cups in the wilderness measuring points were 0.3, 0.5, 1.0, 1.5, and 2.0 m. The heights of the wind cup at the other measuring points were 0.1, 0.2, 0.3, and 0.5 m (Figure 9). The observation step of the wind speed was 10 s, the observation time of each measuring point was not less than 30 min, and the measured wind speed was instantaneous.

4.4.3 Verification of wind-proof effect in the field

Figure 10 shows the change in the wind-proof effect at the height of 0.2 m near the surface of nine configurations of double-row wing bag sand barriers with 4 m spacing at different positions and under the action of wind speed of 6.06, 8.50, and 10.07 m/s. As the airflow gradually approached the wing bag sand barrier, the inflection point was developed at −4H. The sand barrier exerted a protective effect

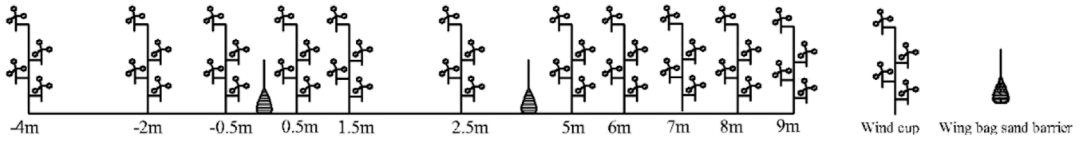

FIGURE 9
Schematic diagram of field wind cup measuring point layout.

and achieved the best wind protective effect as the airflow passed through the first row of sand barriers and gradually decreased as the airflow moved away from the sand barrier. The Windbreak effect increased steadily before the second row of the wing bag sand barrier, then decreased and gradually returned to the initial state. The overall wind proof effect was an "M" shape. In the wilderness, the increase in the wind speed weakened the wind proof effect of the same wing bag sand barrier. However, the wind proof effect law remained unchanged with the change in the wind speed.

When the wind speed was 6.06 m/s, the effective protection range behind the sand barrier with nine modes of specifications was more than 7.77 m. Among which the protective effect by the wing bag sand barrier having the specifications of 25 cm × 20 cm (10.43 m), 30 cm × 20 cm (9.78 m), and 25 cm × 25 cm (9.43 m) showed a better protective effect compared to the other modes. When the wind speed was 8.50 m/s, the three-wing bag sand barrier mode having a bottom bag diameter of 25 cm was the best. When the wind speed increased to 10.07 m/s, the effective protection distances of the sand barriers with specifications of 25 cm × 25 cm, 20 cm × 30 cm, and 25 cm × 20 cm were 8.91, 8.16, and 8.10 m, respectively, which were better than that of the other sand barriers. However, from the perspective of protective effect (Table 5), at the wind speed of 10.07 m/s, the protective effect of the wing bag sand barriers with specifications of 20 cm × 30 cm, 20 cm × 25 cm, and 25 cm × 30 cm showed a better protective effect at 8H on the leeward side and was accounted for 77.40%, 69.15%, and 65.76%, respectively. The protective effect of the three specifications with the bottom band diameter of 30 cm was relatively poor. The results of the wind tunnel simulation experiment were consistent with those of the field experiment.

5 Discussion

5.1 Air velocity characteristics of wing bag sand barrier

The wing bag sand barrier is a combination of both dynamic and static sand fixation methods and has a "wing" added to the conventional bag sand barrier, which can fluctuate with the wind. The inclusion of a wing in the sand barrier can eliminate the wind, thereby increasing the resistance of sand wind and slowing down the sand wind layer by layer. This process facilitates fixing sand in the bottom bag, thereby improving the effect of wind prevention and sand fixation. The wing bag sand barrier can increase the wind protective effect by an average of 48% compared with the conventional banded sand barrier (without wings) (Gao et al., 2019) and the effective protection distance by 14.24H–41.70H (Han, 2022). During operation, the fluctuating wing has a significant effect on the wind speed. The wing part of the wing bag sand barrier used in this study was made up of airtight material. Consequently, the near-surface airflow formed a reverse vortex at different degrees in and behind the double-row wing bag sand barrier. When the reverse vortex collided with the incoming flow, the airflow weakened, forming a low-speed/calm wind zone in and behind the sand barrier. This phenomenon is similar to that of the conventional airtight sand barrier; however, the dynamic wing has a better wind energy weakening effect. In the wing bag sand barrier, both the scope of the leeward static wind zone and the thickness of the near-surface static wind layer of the wing have been improved compared to the conventional airtight sand barrier (Yuan et al., 2019; Yan et al., 2021).

The wing bag sand barriers with different specifications have an effective protection distance between 1 and 2.5H before the sand barrier, indicating that the wing swing also has a certain interference effect on the airflow. The protection area of the sand barrier of the wing bag decreased by 2–4H with the increase in the wind speed in the same configuration mode; however, the trend of the horizontal airflow field remained unchanged, indicating that the fluctuation of wind speed has no significant influence on the change law of the airflow field. Although the disturbance effect of the wing on the wind speed has a certain value, it also remained unaffected by the increase in the wind speed. The sand barrier specification effect was better for bottom bag diameter of 12.5 and 10 cm than that of 15 cm at three wind speeds, indicating a better effect as the specification increases. If the wing is too high, it can easily dislodge and affect the effective protection area behind the barrier. Bandwidth spacing is a key factor affecting the wind-proof effect of the double-row sand barrier. When spacing is too narrow, the protective benefit areas in the barrier can be overlapped, and when spacing is broad areas without protective benefits can be developed (Zhang et al., 2005; Jia, 2019; Li et al., 2019; Chen et al., 2020; Jia et al., 2020; Xi et al., 2021). In this study, the windbreak effect of the sand barrier was in the order of 2 m > 1.5 m > 1 m. In future research, the optimal distance between double-row wing bags and the maximum protection benefit can be achieved by modifying the bandwidth spacing. Han (2022) evaluated the impact of single and double rows of the wing bag sand barrier on sand resistance and showed that the protection range of the double row of the wing bag sand barrier could be increased by 1.04–1.96 times compared with the single row of the wing bag sand barrier. According to Xi's research on the protective benefit characteristics and optimal configuration of nylon sand fixation barrier, the double sand barrier has significantly improved the sand blocking ability compared with the single sand barrier (Xi, 2022).

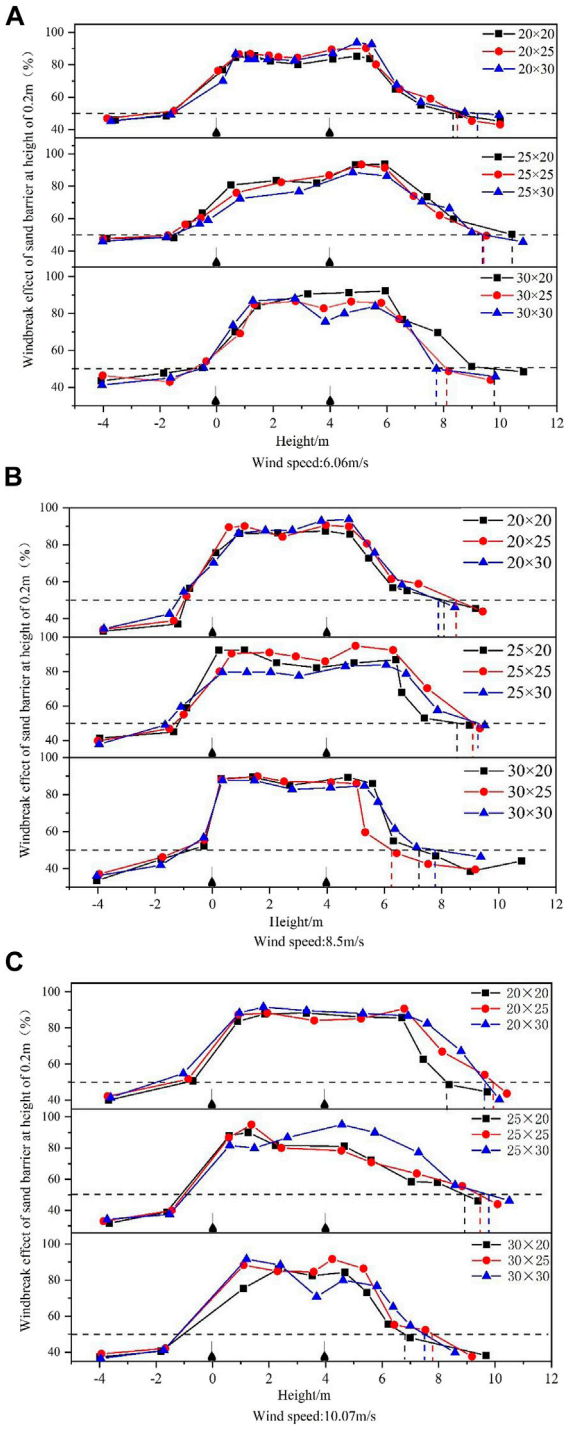

FIGURE 10
Field windbreak effect of double-row wing bag sand barrier dune and the direction of movement.

Wang et al. (2008) measured the influence of nine kinds of ribbon sand barriers on wind speed, surface roughness, and near-surface sediment transport rate. The best effect was shown in the three-line belt with a height of 1.5 m and spacing of 1.5 and 10.5 m. The second best was a two-line belt with a height of 1.5 m, spacing of 1.5 and 7.5 m. The third was a three-line belt with a height of 1 m, spacing of 1, and 7 m. Therefore, Single line sand barriers, regardless of height, are not cost-effective (Wang et al., 2008). In practical application, the number of sand barrier rows determines the effectiveness of the sand barrier to a large extent. The best effect cannot be achieved with a few sand barrier rows. Conversely, a greater number of rows will increase the cost. Therefore, a low-cost sand barrier mode that provides benefits using fewer materials should be selected to obtain maximum output. The wind tunnel simulation pre-test on the wind and sand preventing effect of single-row, double-row, and triple-row wing bag sand barriers, showed that both double-row and triple-row wing bag sand barriers had better wind and sand preventing effects. Nevertheless, the double-row wing bag sand barrier was shown to be the best sand control mode when considering both wind and sand preventing effect and cost input.

5.2 Wing bag sand barrier wind sand flow structure characteristics

Based on the vertical distribution of wind-sand flow, the sediment transport per unit time per unit area was in the order of cavity > in the barrier > behind the barrier. The change in wind speed has a significant effect on sediment transport. At constant wing bag sand barrier size, the total sediment volume and sediment height increased gradually with the increase in wind speed. Previous research on the motion characteristics of aeolian sand flow shows that the sand content in the aeolian sand flow decreases with the increase of vertical height. A majority of the sand particles are transported within 30 cm near the ground, mainly in the airflow of 0–10 cm, and the increase of wind speed significantly increases the sediment transport (Chepil and Woodruff, 1957; Luo et al., 2019). According to Mao (2011), the amount of sediment transported within 30 cm height accounted for 64%–83% of the total amount of sediment transported. A study by Zhang et al. (2004) in Tengger Desert showed 96% of total sediment transport in the height range of 10 cm from the surface. Xu et al. (2013) reported 70% of total sediment transport within the height below 10 cm on the surface of the mobile dune in the Ulan Buh Desert. According to their study, the movement of wind-blown sand is a process of sand transport close to the surface (Xu et al., 2013).

Similarly, in this study, a significant effect on intercepting the sand load of the wind-blown sand flow below 20 cm was observed by setting the wing bag sand barrier with the diameter and height of the bottom bag of 20–30 cm. The difference observed in this study compared to the previous studies is that the wind-blown sand flow was affected by the wing bag sand barrier, which changed the original law and characteristics. The sand content in wind-blown sand flow decreased with the increase in vertical height. More than 81% of sediment transport in and after the barrier was distributed in the 0–10 cm when the wind speed was 6 m/s. When the wind speed was 12 m/s, sediment transport in the barrier accounted for only 28% of the 0–10 cm height. This was due to blocking the strong airflow carrying sand by the sand barrier when it was being passed through the wing bag sand barrier in a short time. As the sand-carrying airflow gradually raised, sediment transport at the height of 0–10 cm gradually decreased in and after the barrier. However, the amount of sediment transported above 10 cm increased gradually, and in the 30–60 cm height layer, the wind-blown sand flow raised

TABLE 5 Different specifications of wing bag sand barrier field wind-proof effect (indicating wind speed of 10.07 m/s).

Model specification (cm × cm)	WSBB ($m·s^{-1}$)	WSIB ($m·s^{-1}$)	WSAB ($m·s^{-1}$)	WE (%)
20 × 20	8.16	2.68	4.60	54.36
20 × 25	8.20	1.78	3.11	69.15
20 × 30	8.06	1.40	2.28	77.40
25 × 20	8.19	3.92	4.26	57.65
25 × 25	8.16	2.6	4.05	59.77
25 × 30	8.25	0.6	3.45	65.76
30 × 20	8.26	3.26	5.60	44.35
30 × 25	8.19	1.00	5.22	48.16
30 × 30	8.18	4.6	5.51	45.26

Note: WSBB, denotes the wind speed 5H before the barrier; WSIB, denotes the wind speed 4H in the barrier; WSAB, denotes the wind speed 10H after the barrier; WE, denotes the wind-proof efficiency.

twice after the second row of sand barriers. This was due to the wind-proof property of sand barrier material, which led to noticeable air uplift at high wind speed. Some scholars have used wind tunnel simulation to show the direct effect of nylon net sand barriers with different porosity on the penetration ability of sand particles (Zhang et al., 2004). They further stated that the nylon net sand barriers with different porosity also changed the turbulent characteristics of the airflow, which has a crucial impact on the protection benefits of sand barriers (Zhang et al., 2004).

The porosity of wings can change the overall wind-proof and sand-fixing effect of sand barriers. The effect of the wing bag sand barrier on sand grains in the 0–10 cm and 10–30 cm height layers was to block the leeward side of the barrier, and the effect of 30–50 cm and 50–60 cm height layers was to transport the sand grains, which is consistent with the research results of Yan et al. (2021). The interception rate in the 0–30 cm height layer decreased as the wind speed increased, while the conductivity in the 30–60 cm height layer steadily increased, indicating that the change in wind speed plays a dominant role in sand barrier interception rate/conductivity. In addition, Gao's research team has already explained the surface erosion around the wing bag sand barrier (Gao, 2021). Their field and wind tunnel simulation experiments using the wing bag sand barrier with different specifications showed wind erosion before the sand barrier and accumulation of sand after the sand barrier. These results suggested effective sand fixation by wing bag sand barrier and reduced erosion of the sand surface by the wind.

5.3 Prospect

Conventional static sand-fixing can change into dynamic sand-fixing by lifting the sand barrier when the sand barrier is buried by quicksand. Hence, the theory of "the barrier grows with the sand, and the sand grows with the barrier" can be achieved. Therefore, dynamic sand fixation and dynamic-static sand fixation modes will be the new trends in the next few years.

The wind tunnel experiment is the commonly used simulation method to regulate experimental conditions more accurately. Moreover, wind tunnel experiment results are highly precise, and the experiment process is safer, with high efficiency and low cost. However, there are some limitations. The airflow in the wind tunnel test is DC down-blowing, which can well reflect the airflow variation around the sand barrier under a single wind direction. Nonetheless, there are some errors in the simulation of the airflow field of the sand barrier with a grid wing bag suitable for multiple wind directions. In future studies, the mode and specification of the wing bag sand barrier should be adjusted and tested in the field under windy conditions to fill the blank of the wing bag sand barrier under multi-wind conditions. Long-term monitoring studies on the vegetation coverage of the field study area should be combined with remote sensing interpretation methods (Huang et al., 2020a; Huang et al., 2020b; Huang et al., 2020c). Furthermore, the effect of the wing bag sand barrier on windbreak and sand fixation should be verified laterally.

6 Conclusion

The wing bag sand barrier is a new type of sand barrier with the advanced technology, breaking the single sand-fixing mode of the mechanical sand barrier for the first time. To select the best configuration mode of the wing bag sand barrier under different wind conditions, this paper compared and analyzed the wind-proof and sand-fixing effects of the double-row wing bag sand barrier with nine configuration modes. The findings are as follows:

(1) For the same specifications, the range of weak or still wind area on the leeward side of the wing bag sand barrier decreased with the increase in wind speed. At three wind speeds, the effective protection range of sand barriers was better for the sizes of 10 cm × 15 cm and 12.5 cm × 10 cm than that of the other specifications, and an optimal protective effect was observed when the bandwidth was 2 m.
(2) When the wind speed was less than 8 m/s, sand accumulation in and behind the barrier was mainly concentrated in the 0–10 cm height layer. As the wind speed reached 12 m/s, sand accumulation was significant in the 30–60 cm height layer,

and behind the barrier, it was 58%–82% in the same height layer. Sand transport could be reduced by 21%–95% in the front row when airflow was affected by the sand barrier compared with that in the hollow. Sand transport could be reduced by 68%–99% in the second row when airflow passed through the sand barrier, and the sand resistance effect was apparent.

(3) The effects of the 0–30 cm layer and the 30–60 cm layer of the sand barriers on the sand particles were shown as interception and transport, respectively. With the increase in wind speed, the interception rate decreased while the conductivity decreased. At different wind speeds, the average retention rates of sand barriers with the specification of 12.5 cm × 12.5 cm were 94% at 0–30 cm height and 96% at 30–60 cm height, which were better than the specifications of 12.5 cm × 15 cm and 12.5 cm × 10 cm.

(4) In the field, at wind speeds less than 6 m/s, the recommended specifications of the wing bag sand barrier were 25 cm × 20 cm or 30 cm × 20 cm. At an inlet wind speed of 8 m/s, the recommended specifications were 25 cm × 20 cm and 25 cm × 25 cm. When the wind speed was greater than 12 m/s, specifications of 25 cm × 25 cm, 25 cm × 20 cm, and 20 cm × 25 cm were recommended.

Data availability statement

The original contributions presented in the study are included in the article/supplementary material, further inquiries can be directed to the corresponding author.

Author contributions

X-YH wrote the main manuscript text, and G-PJ prepared Figures 1–10. In addition, JL and YY reviewed and revised the manuscript. T-XG processes the wind tunnel data. All authors discussed the results and commented on the manuscript.

Funding

This study was supported by the Natural Science Foundation of Inner Mongolia Autonomous Region Science and Technology Major Project (2019ZD003-3).

Conflict of interest

The authors declare that the research was conducted in the absence of any commercial or financial relationships that could be construed as a potential conflict of interest.

Publisher's note

All claims expressed in this article are solely those of the authors and do not necessarily represent those of their affiliated organizations, or those of the publisher, the editors and the reviewers. Any product that may be evaluated in this article, or claim that may be made by its manufacturer, is not guaranteed or endorsed by the publisher.

References

Bai, M. (2009). *Application of geosynthetic materials in the control of sand damage along Jiangbei Highway in Shannan area of Xizang Province*. China: Chongqing Jiaotong University.

Chang, Z. F., Zhong, S. N., and Han, F. G. (2000). Research on the reasonable spacing of clay sand barrier and wheat grass sand barrier. *J. Desert Res.* 20 (4), 111–113. doi:10.00-694X/(2000)04-0455-03

Chen, B. Y., Cheng, J. J., and Li, S. Y. (2020). Analysis on the reasonable spacing of tall reed sand barriers on Provincial Highway S214 in. *Xinjiang Arid Zone Res.* 37 (03), 782–789. doi:10.13866/j.azr.2003.28

Chepil, W. S., and Woodruff, N. P. (1957). Sedimentary characteristics of dust storms (Part II): Visibility and dust concentration. *Am. J. Sci.* 255 (02), 104–114. doi:10.2475/ajs.255.2.104

Dong, Z., Li, H. L., Wang, J., Guangtian, S., Zhang, J., et al. (2007). Wind tunnel simulation experiment on windbreak effect of geogrid sand barrier. *Sci. Soil Water Conservation* (01), 35–39. doi:10.16843/j.sswc.2007.01.008

Dong, Z. (2004). *Research on farmland wind-sand disaster of oasis and its control mechanism in ulan Buh Desert*. Beijing: Beijing Forestry University.

Gao, T. X., Wang, T., Yang, W. B., Guangtian, Shi, and Zhang, J. (2019). Wind tunnel experiment on windbreak and sand accumulation effect of low-coverage wing bag sand barrier. *J. Desert Res.* 39 (06), 177–183. doi:10.7522/j.issn.1000-694X.2019.00073

Gao, T. X. (2021). Wind tunnel simulation study on Mechanism of windbreak and sand fixation of wing bag sand barrier. *Inn. Mong. Agric. Univ.*, doi:10.27229/d.cnki.gnmnu.2021.001058

Gao, Y., Yang, H., Dong, J., Zhang, M., Gao, X., Zhang, J., et al. (2022). Growth and photosynthesis responses of microcystin (MC)- and non-MC-producing Microcystis strains during co-culture with the submerged macrophyte Myriophyllum spicatum. *J. Inn. Mong. Agric. Univ. Nat. Sci.* 43 (05), 56–65. doi:10.2166/wst.2022.166

Guo, X. N. (2021). Desertification in Mongolian Plateau in recent 20 years: Evolutional trend, driving mechanism, and ecological effects. *East China Norm. Univ.* 56 (2004), 449–464. doi:10.27149/d.cnki.ghdsu.2021.000315

Han, X. Y., Wang, T., Yang, W. B., Guangpu, J., Jing, L., and Yang, Yu (2021a). Research progress and hotspot analysis of sand barrier in China: Quantitative analysis of atlas based on Vosviewer and Citespace. *J. Desert Res.* 41 (02), 153–163. doi:10.7522/j.issn.1000-694X.2020.00117

Han, X. Y., Yang, W. B., and Hu, H. (2021b). *A Wind-feathered Bag sand barrier*. Beijing: CN213508400U.

Han, X. Y. (2022). Wing bag barrier protection mechanism and sand benefit research. *Inn. Mong. Agric. Univ.* Doctoral Dissertation, doi:10.27229/,dcnki.Gnmnu.2022.000063

Hu, C. Y., Yang, M., and Yang, C. L. (2002). Comprehensive control technology of sand hazard on the highway through sand in Kubuqi Desert. *J. Arid Land Resour. Environ.* (03), 71–77. doi:10.03-7578/(2002)03-071-07

Huang, F. M., Cao, Z. S., Guo, J. F., and Jiang, S. H. (2020a). Comparisons of heuristic, general statistical and machine learning models for landslide susceptibility prediction and mapping. *CATENA* 191, 104580. doi:10.1016/j.catena.2020.104580

Huang, F. M., Cao, Z. S., Jiang, S. H., Zhou, C., Huang, J., and Guo, Z. (2020b). Landslide susceptibility prediction based on a semi-supervised multiple-layer perceptron model. *Landslides* 17, 2919–2930. doi:10.1007/s10346-020-01473-9

Huang, F. M., Zhang, J., Zhou, C. B., Wang, Y., Huang, J., and Zhu, L. (2020c). A deep learning algorithm using a fully connected sparse autoencoder neural network for landslide susceptibility prediction. *Landslides* 17 (01), 217–229. doi:10.1007/s10346-019-01274-9

Jia, G. P., Zuo, H. J., and Yan, M. (2020). Different heights of the double line of nylon resistance sand network reasonable spacing study. *J. Resour. Environ. Arid Areas*. 1, 132–139. doi:10.13448/j.carol.carroll.nki.jalre.2020.018

Jia, G. P. (2019). Numerical simulation of protective effect of two-row nylon sand-blocking net by Fluent. *Inn. Mong. Agric. Univ.*, Master Dissertation. doi:10.27229/d.CNKI.GNMNU.2019.000354

Li, J. Y., Tohti, I. A., and Yumati, W. (2020). Sand control effect of low vertical gravel barrier in Xinjiang. *Soil Water Conservation China* 2021 (10), 42–44. doi:10.14123/J.CNKI.SWCC2021.0247

Li, K. C., Tan, L. M., and Shi, L. (2022). Influence of porosity on blown sand protective effect of reed sand barrier. *J. China Railw. Soc.* 44 (05), 166–170. doi:10.01-8360/(2022) 05-0166-05

Li, K. C., Zhou, Q., and Ding, L. S. (2019). Wind-blown sand protection mechanism and effect evaluation of HDPE sand barrier in Gobi District of South Xinjiang. *China Railw. Sci.*, ,40(03): 10–14. doi:10.01-4632/(2019)03-0010-05

Liang, Y. M., Gao, Y., and Dang, X. H. (2022). Characteristics of erosion and fungal community in sand buried parts of sand barrier of Salix. *Chin. J. Appl. Environ. Biol.* 28 (02), 339–345. doi:10.19675/j.cnki.1006-687x.2020.11037

Liu, L. (2008). *Research on wind erosion control benefit of mechanical sand barrier on qinghai-tibet railway*. Beijing: Beijing Jiaotong University.

Luo, F. M., Gao, J. L., and Xin, Z. M. (2019). Characteristics of sand-driving wind regime and sediment transport in northeast edge of Ulan Buh Desert. *Trans. Chin. Soc. Agric. Eng. Trans. CSAE)* 35 (4), 145–152. doi:10.11975/j.issn.1002-6819.2019. 04.018

Luo, J. B. (2005). *Study on techniques and its mechanism of controlling sand hazard to highway in different type regions of Desert in China*. Beijing: Beijing Forestry University.

Mao, D. L. (2011). Research on wind-sand structure of foreland of wind-sand in oasis-desert ecotone in cele area. *Mod. Agric. Sci. Technol.* (15), 266–269.

Mcewan, I. K., and Willetts, B. B. (1993). Adaptation of the near-surface wind to the development of sand transport. *J. Fluid Mech.* 252, 99–115. doi:10.1017/ s0022112093003684

Meng, Z. J., Ren, X. M., and Gao, Y. (2014). Effect of semi-hidden sand barrier on wind and sand resistance of Salix. *Bull. Soil Water Conservation* 34 (3), 178–180+206. doi:10.13961/j.cnki.stbctb.2014.03.034

Miao, R. H., Guo, M. X., and Liu, Y. Z. (2018). Effects of different biological sand barriers on vegetation restoration and soil moisture in Horqin Mobile Dune. *J. Ecol. Environ.* 27 (11), 1987–1992. doi:10.16258/J.CNKI.1674-5906.2018.11.002

Neuman, M. K., Sanderson, R. S., and Sutton, S. (2013). Vortex shedding and morphodynamic response of bed surface containing non-erodible roughness elements. *Geomorphology* 198, 45–46. doi:10.1016/j.geomorph.2013.05.011

Nie, L. G. (2012). Analysis of sand blown prevention mechanism in inner Mongolia. *J. Railw. Eng.* 29 (10), 31–36. doi:10.06-2106/(2012)10-0031-06

Qiu, G. Y., Shimizu, H., Gao, Y., and Ding, G. (2004). Principles of sand dune fixation with straw checkerboard technology and its effects on the environment. *J. Arid Environ.* 56 (3), 449–464. doi:10.1016/S0140-1963(03)00066-1

Qu, J. J., Yu, W. B., and Qin, X. B. (2014). Wind-protecting efficiency of HDPE functional sand-fixing barriers. *J. Desert Res.* 34 (5), 1185–1193. doi:10.7522/j.issn.1000-694X.2013.00446

Shi, L., Zhao, Y. X., Haselton, E., Yingjun, X., and Zhuoran, W. (2021). Changes of vegetation and soil nutrients on windward slope of dune under sand barrier environment in Mu Su sandy land. *J. Desert Res.* 41 (05), 140–146. doi:10.7522/j. issn.1000-694X.2021.00051

Sun, T., Liu, H. J., and Zhu, G. Q. (2012). Time-effectiveness of three mechanical sand barriers for windbreak and sand fixation. *J. Soil Water Conservation* 26 (4), 12–16+22. doi:10.13870/j.cnki.stbcxb.2012.04.051

Wang, J. B., Cui, Y. C., and Zhang, Q. Y. (2021). Study on the influence of wind speed on sand control effect of grass grid sand barrier. *Soil Water Conservation China* 2021 (12), 44–46. + 7. doi:10.14123/J.CNKI.SWCC2021.0294

Wang, Q., Zuo, H. J., and Li, G. T. (2018). Study on the efficiency of windbreak and sand fixation for the stubble sand barrier of macrofungi and its suitable model. *Arid Zone Res.* 35 (05), 1234–1241. doi:10.13866/j.azr.2018.05.29

Wang, T., Qu, J. J., and Niu, Q. H. (2020). Comparative study of the shelter efficacy of straw checkerboard barriers and rocky checkerboard barriers in a wind tunnel. *Aeolian Res.* 43, 100575. doi:10.1016/j.aeolia.2020.100575

Wang, X. Y., Ding, G. D., and Gao, H. (2008). Study on windbreak and sand fixation efficiency of ribbon sand barrier. *J. Soil Water Conservation* (02), 42–46. doi:10.13870/j. cnki.stbcxb.2008.02.003

Wu, J. Y. (2009). *Study on effects and mechanism on the integrated controlling sand hazard to highway in otindag sandy land*. China: Inner Mongolia Agricultural University.

Wu, Z. (2003). *Aeolian geomorphology and sand control Engineering*. Beijing: Science Press, 331–334.

Wu, Z., Dong, Z. B., and Li, B. S. (2003). *Geomorphology and sand control engineering*. Beijing: Science Press.

Xi, C. (2022). Nylon sand-fixation resistance of sand barrier protection efficiency characteristic and optimizing the allocation of research. *Inn. Mong. Agric. Univ*. Master Dissertation, doi:10.27229/,dcnki.Gnmnu.2022.001005

Xi, C., Zuo, H. J., and Wang, H. B. (2021). Nylon mesh barrier high vertical wind resistance of sand characteristics and reasonable configuration. *J. Res. Arid Areas* 38 (03), 882–891. doi:10.13866/j.azr.2021.03.30

Xu, B., Zhang, J., Huang, N., Gong, K., and Liu, Y. (2018). Characteristics of turbulent aeolian sand movement over straw checkerboard barriers and formation mechanisms of their internal erosion form. *J. Geophys. Res. Atmos.* 123 (13), 6907–6919. doi:10.1029/ 2017JD027786

Xu, J., Zhang, Y. X., Hao, Y. G., Monterosso, J., Worhunsky, P. D., et al. (2013). Task-related concurrent but opposite modulations of overlapping functional networks as revealed by spatial ICA. *Chin. Agric. Sci. Bull.* 29 (19), 62–71. doi:10.1016/j.neuroimage. 2013.04.038

Yan, M., Zuo, H. J., Guo, Y., Guangtian, S., and Jie, Z. (2021). Wind tunnel simulation of wind-proof and sand-retaining wall under aeolian sand environment. *J. Beijing For. Univ.* 43 (05), 108–117. doi:10.12171/j.1000−1522.20200339

Yang, W. B., Li, W., and Feng, W. (2017). *Low cover wing bag sand barrier*. Beijing: CN107034871A, 2017-08-11.

Yang, W. B. (2016). *Sand control with low coverage: Principle, model and effect*. China: Science Press.

Yuan, L. M., Huang, H. G., and Yan, D. R. (2019). Study on the effect of ribbon sand barrier on windbreak and sand fixation under different degrees of sand burial. *Trans. CSAE* 35 (16), 172–179. doi:10.19675/j.cnki.1006-687x.2020.11037

Zhang, K. C., Qu, J. J., and Zu, R. P. (2005). Simulation on abated effect of nylon and plastic nets with different structures on wind-blown sand in wind tunnel. *J. Desert Res.* 25 (4), 483–487.

Zhang, K. C., Qu, J. J., and Zu, R. P. (2004). Wind tunnel simulation to determine the effect of underlying sand-laden layer surface characteristics on air current turbulence. *Bull. Soil Water Conservation* 24 (3), 1–4. doi:10.13961/j.cnki.stbctb. 2004.03.001

Zhang, W. M., Tan, L. H., and Zhang, K. C. (2012). Field wind tunnel experiment on bed erosion process with different gravel coverage. *Sci. Geogr. Sin.* 32 (11), 1370–1376. doi:10.13249/j.cnki.sgs.2012.11.012